Dispersion-managed mode-locking dynamics in a Ti:sapphire laser

Marco V. Tognetti,* Miguel N. Miranda, and Helder M. Crespo
CLOQ/Departamento de Física, Faculdade de Ciências, Universidade do Porto, Rua do Campo Alegre 687, 4169-007 Porto, Portugal
(Received 3 March 2006; published 12 September 2006)

We present what is to our knowledge the most complete one-dimensional numerical analysis of the evolution and the propagation dynamics of an ultrashort laser pulse in a Ti:sapphire laser oscillator. This study confirms the dispersion managed model of mode locking, and emphasizes the role of the Kerr nonlinearity in generating mode-locked spectra with a smooth and well-behaved spectral phase. A very good agreement with experimental measurements of pulse energy, spectrum, and temporal width of extracavity compressed pulses is found.

DOI: 10.1103/PhysRevA.74.033809 PACS number(s): 42.65.Tg, 42.60.Fc, 42.65.Re, 42.55.Ah

I. INTRODUCTION

Pulse generation in mode-locked lasers has been a subject of intense research over more than two decades. In more recent descriptions of Kerr-lens mode-locked (KLM) ultrafast lasers, pulse formation is assumed to rely upon a solitonlike mechanism, based on the master equation approximation [1], where the combined and balanced action of self-phase modulation (SPM) and group-delay dispersion (GDD) is the basis for the generation of a short pulse. In this picture the shortest pulse durations are obtained for cavity configurations with minimum net GDD. This approach gives a good description of actual systems but relies on the assumption that changes in the pulse parameters for each round trip are small. Furthermore, it does not take into account the pulse propagation dynamics in the individual optical elements that comprise a laser cavity and usually does not include higher order dispersion terms, which are known to significantly affect sub-10-fs pulses such as those generated with today's state-of-the-art laser oscillators [2,3]. The inclusion of third-order dispersion nevertheless allowed to describe important phenomena such as spectral splitting and dispersive wave generation [4]. As an alternative to the master equation approach, the evolution of laser pulses has also been modeled numerically [5,6], but the actual sequence of intracavity components was not taken into consideration. In fact, the arrangement of the optical elements is actually crucial in describing the steady-state intracavity propagation dynamics, as the pulse assumes different spectral and temporal profiles in different oscillator regions due to the *discrete* nature of ultrafast optical cavities. This makes pulse propagation dynamics deviating from pure solitonlike behavior [7–9]. Also, strong variations in dispersion, as first obtained in a stretched-pulse mode-locked fiber laser [10], can result in bandwidth enhancement and efficient suppression of instabilities—namely, spectral sidebands—with respect to pure solitonlike operation [11]. In this view, a new model for the generation of ultrashort pulses was later introduced by Chen *et al.* [12] directly related to the nonlinear propagation of pulses in dispersion managed communication fibers. They identify a solid state mode-locked laser as another example of a system where dispersion managed solitons (DMS) can be observed. DMS are stable solitonlike solutions of the nonlinear Schrödinger equation which are known to occur in optical media with a periodical change of sign in the GDD [13], such as a femtosecond laser cavity. The main difference from *standard* soliton propagation is that the spectrum and temporal profile of DMS periodically broaden and recompress as the pulse crosses regions of opposite GDD. This elegant yet simple model allows one to determine the general features of the steady state pulse propagation, namely, the pronounced soliton breathing and flattened spectral shape that occur under strong SPM conditions. However, it assumes a perfectly symmetric and steplike GDD distribution, which is an approximation of actual KLM linear laser cavities, and it does not consider the actual pulse evolution from initial noise, assuming instead steady-state solutions with an *a priori* flat spectral phase. Even though a study has been performed that relates laser pulse energy and temporal width in the light of the DMM model [14], to the best of our knowledge no detailed and quantitative comparison of this model with actual experimental measurements has yet been performed.

Here we present what is to our knowledge the most detailed one-dimensional (1D) numerical simulation of a prism-dispersion controlled linear laser cavity, which includes build up of the laser pulse from noise through the action of active- and Kerr-lens mode locking, the measured reflectivity and phase distortion of every optical element in the cavity, the measured gain bandwidth of the Ti:sapphire crystal, and the propagation inside the active medium, by numerically solving the corresponding nonlinear Schrödinger equation in the presence of gain. In particular, great attention is devoted to intracavity pulse formation and propagation, showing how the spectrum and its phase evolve as the pulse crosses the crystal, is reflected off the intracavity mirrors, and goes through the negatively dispersive prism line. This model not only confirms the dispersion managed model of mode locking, but also accurately reproduces the behavior and characteristics of the generated pulses measured outside the laser cavity and appears to be a very helpful numerical instrument in predicting the performance of actual experimental devices.

II. MODEL DESCRIPTION

Figure 1(a) shows a schematic diagram of the Ti:sapphire laser oscillator. This system has been described elsewhere

*Electronic address: marco.tognetti@fc.up.pt

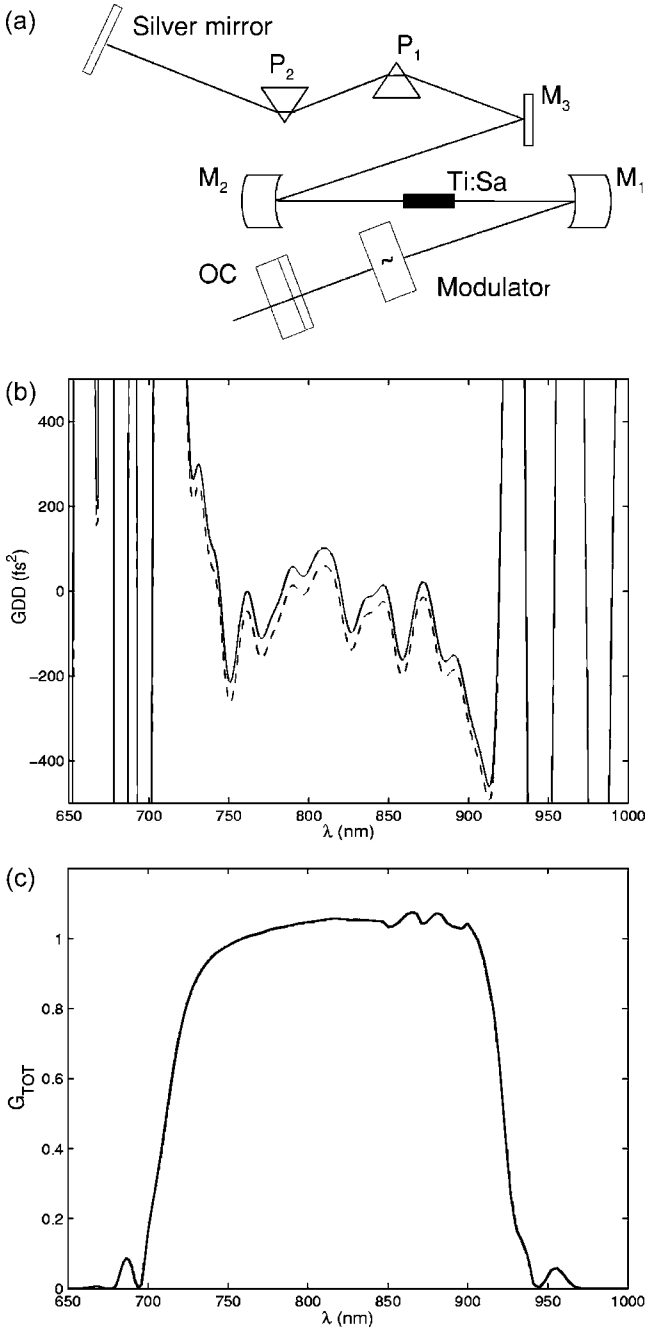

FIG. 1. (a) Schematic diagram of the Ti:sapphire laser oscillator. (b) Total round trip intracavity GDD (dashed line corresponds to less prism insertion). (c) Total cavity gain G_{tot} assuming a peak crystal gain of 1.04.

[15], and consists of an active crystal of length L enclosed between two focusing mirrors M_1 and M_2, a flat folding mirror M_3, an output coupler (OC) and a silver high reflector at the cavity ends, a pair of fused-silica prisms for dispersion compensation, and an active amplitude modulator $M(t)$ to form the initial pulse from noise. The evolution of the pulse inside the cavity is described by the following iterative procedure which connects the spectral amplitude of the field, $\tilde{A}_{k+1}(\omega)$, for the $(k+1)$-th passage inside the cavity, with the field envelope $A_k(t)$, obtained from the previous passage:

$$\tilde{A}_{k_1}(\omega) = R_1(\omega)^{1/2} e^{i[\phi_1(\omega)+\phi_{air1}(\omega)]} \int_{-\infty}^{+\infty} M(t) A_k(t) e^{-i\omega t},$$

$$\tilde{A}_{k_2}(\omega) = \mathcal{P}(\tilde{A}_{k_1}(\omega)),$$

$$\tilde{A}_{k_3}(\omega) = R_2(\omega) R_3(\omega) e^{2i[\phi_2(\omega)+\phi_3(\omega)+\phi_{pr}(\omega)+\phi_{air2}(\omega)]} \tilde{A}_{k_2}(\omega),$$

$$\tilde{A}_{k_4}(\omega) = \mathcal{P}(\tilde{A}_{k_3}(\omega)),$$

$$\tilde{A}_{k+1}(\omega) = [R_1(\omega) R_{\mathrm{OC}}(\omega)]^{1/2} e^{i[\phi_1(\omega)+\phi_{\mathrm{OC}}(\omega)+\phi_{\mathrm{air3}}(\omega)]} \tilde{A}_{k_4}(\omega), \tag{1}$$

where R_i and ϕ_i are the reflectivity and phase of the ith optical element, including the contribution of the actual air path between each component, $M(t)$ is an initial active modulation used to start mode-locked operation [5], and $\tilde{A}_{k_{n+1}}(\omega) = \mathcal{P}(\tilde{A}_{k_n}(\omega))$ is the spectral amplitude at the crystal output, obtained by numerically solving the following propagation equation inside the crystal:

$$\frac{\partial A(z,t)}{\partial z} = \int_{-\infty}^{+\infty} [i\beta(\omega) + g(\omega)] \tilde{A}(z,\omega) e^{-i\omega t} d\omega + i\gamma |A(z,t)|^2 A(z,t) \tag{2}$$

with $A(0,t) = A_{k_n}(t)$.

Here $\beta(\omega)$ and $g(\omega)$ are the crystal phase distortion and gain profile per unit length, and $\gamma = 2.2 \times 10^{-6}\ \mathrm{W}^{-1}\ \mathrm{cm}^{-1}$ is the estimated nonlinearity coefficient. Moreover, self-amplitude modulation (SAM) induced by the Kerr nonlinearity is included as a nonlinear intensity discriminator in the time domain [5], here modeled as a super-Gaussian: $K(A) = \exp\{-[(|A| - A_0)/(\sigma A_0)]^m\}$, with $A_0 = \max(|A|)$, $m = 24$, and $\sigma = 0.94$.

These parameters were determined by trial and error, even though the final spectrum will not significantly depend on the exact values, provided that mode-locking operation is established. The crystal gain and the mirror reflectivities and phase distortions were directly obtained from measurements performed on the actual optical components, which comprise a relatively thick (4.5 mm) Ti:sapphire crystal (Crystal Systems, Inc.), commercially available standard ultrafast laser mirrors designed for 850 nm (Spectra-Physics and TecOptics) and a 3.5% output-coupler (Spectra-Physics).

Figures 1(b) and 1(c) show the total GDD and the total cavity gain G_{tot} for one round trip defined as $G_{\mathrm{tot}}(\lambda) = R_1(\lambda)^2 R_2(\lambda)^2 R_3(\lambda)^2 R_{\mathrm{OC}}(\lambda) G(\lambda)^2$, with $G(\lambda) = e^{g(\lambda)L}$ the total crystal gain normalized at 1.04. As initial condition, a *low* amplitude random noise with flat spectral phase is assumed.

III. RESULTS AND DISCUSSION

The evolution of typical intracavity spectral profile and phase of the pulse right before the output coupler are shown in Fig. 2, after (a) 10, (b) 300, (c) 550, and (d) 1000 round trips of the pulse inside the cavity. After the first 10 round

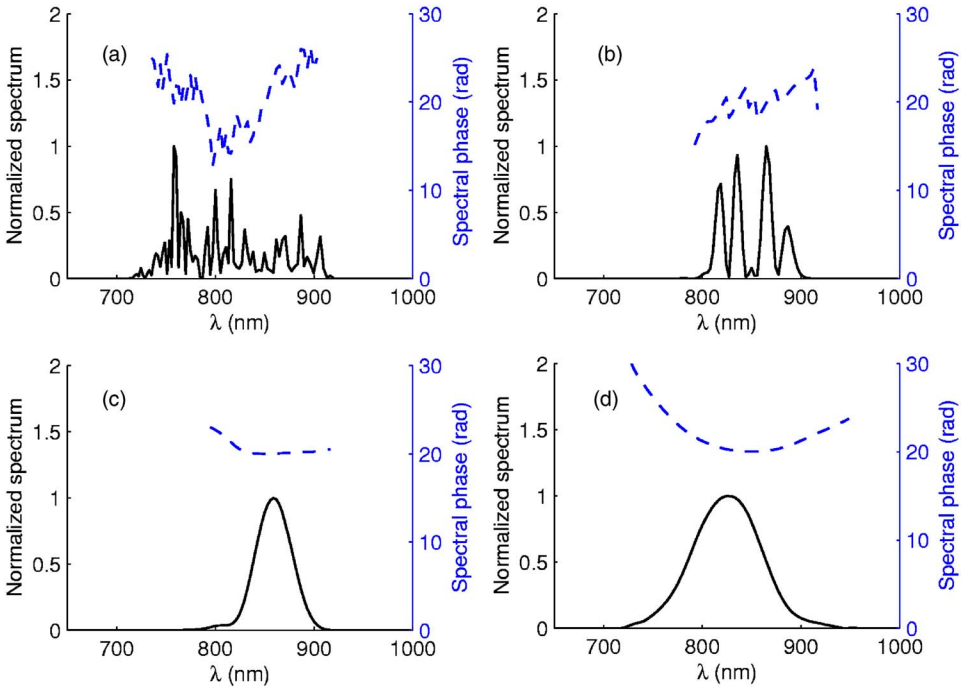

FIG. 2. (Color online) Normalized intracavity spectrum (solid line) and phase (dotted line) before the OC after (a) 10, (b) 300, (c) 550, (d) 1000 round trips inside the cavity.

trips, the spectral phase of the intracavity radiation shows strong fluctuations due to the accumulated linear phase distortion of the optics, as expected from Fig. 1(b). Then a spectrum with increasingly *smooth* spectral phase centered around 850 nm builds up from noise mainly through the action of the crystal gain, the active modulation and SAM, resulting in the spectrum shown in Fig. 2(c) at a pulse peak power of 1.5×10^5 W. As the pulse intensity increases, new mode-locked frequencies are generated via SPM and the spectrum is further broadened until a steady-state is reached at a pulse peak power of 2.7×10^6 W [see Fig. 2(d)], as a result of the interplay between SPM, phase distortion and the finite bandwidth of the total cavity gain [see Fig. 1(c)]. To illustrate the validity of the simulation code the measured and the simulated spectra obtained after the OC are given in Fig. 3, revealing a very good agreement between experimental measurements and theoretical predictions. Also, the model gives a total pulse energy of 1.55 nJ, in excellent agreement with the measured value of 1.49 nJ.

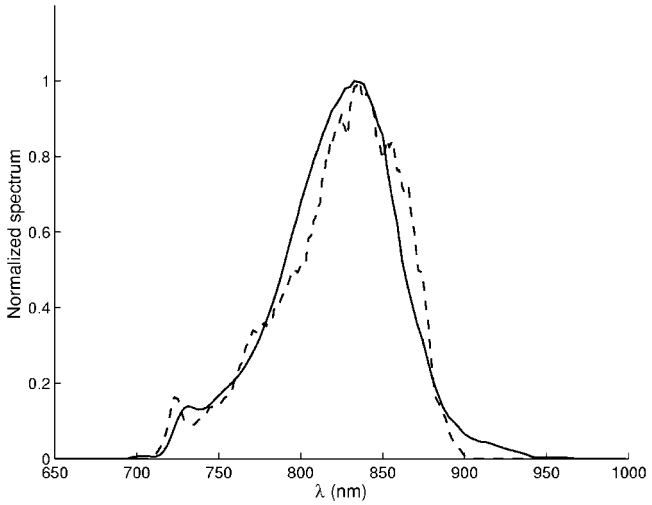

FIG. 3. Simulated (solid line) and measured (dashed line) final spectra outside the OC.

The steady-state spectrum of Fig. 2(d) is reproduced every round trip but it has a different spectral profile in different dispersion regions of the cavity. Figure 4 shows how the cavity can be put in analogy with a dispersion managed fiber made of a region of nonlinear propagation and positive GDD (the active medium crossed two times), and a region of linear propagation and negative GDD (the prism-pair crossed two times).

The OC and the silver mirror are placed in the middle point of each dispersion region. In correspondence with the points A,B,C,D,E, and F of Figs. 4 and 5 shows how the steady-state pulse spectrum, phase, and temporal profile evolve when crossing the crystal, going through the dispersion compensating prism-pair, and coming back to the OC. As the pulse propagates towards the silver mirror, it enters the active medium with a positive chirp (point A in Figs. 4 and 5) and its spectrum broadens while its temporal width increases due to the concomitant action of positive GDD and SPM (points B and C). It can be observed that spectral broadening mainly takes place in the first half of the crystal (from A to B) since temporal broadening due to GDD decreases the strength of SPM as the pulse penetrates more into the crystal. When the pulse crosses the two prisms and

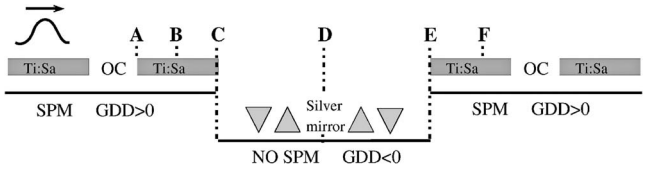

FIG. 4. Laser cavity dispersion map. A,B,C,D,E, and F are reference points corresponding to the spectra, phases, and temporal profiles reported in Fig. 5 (see the text for more details).

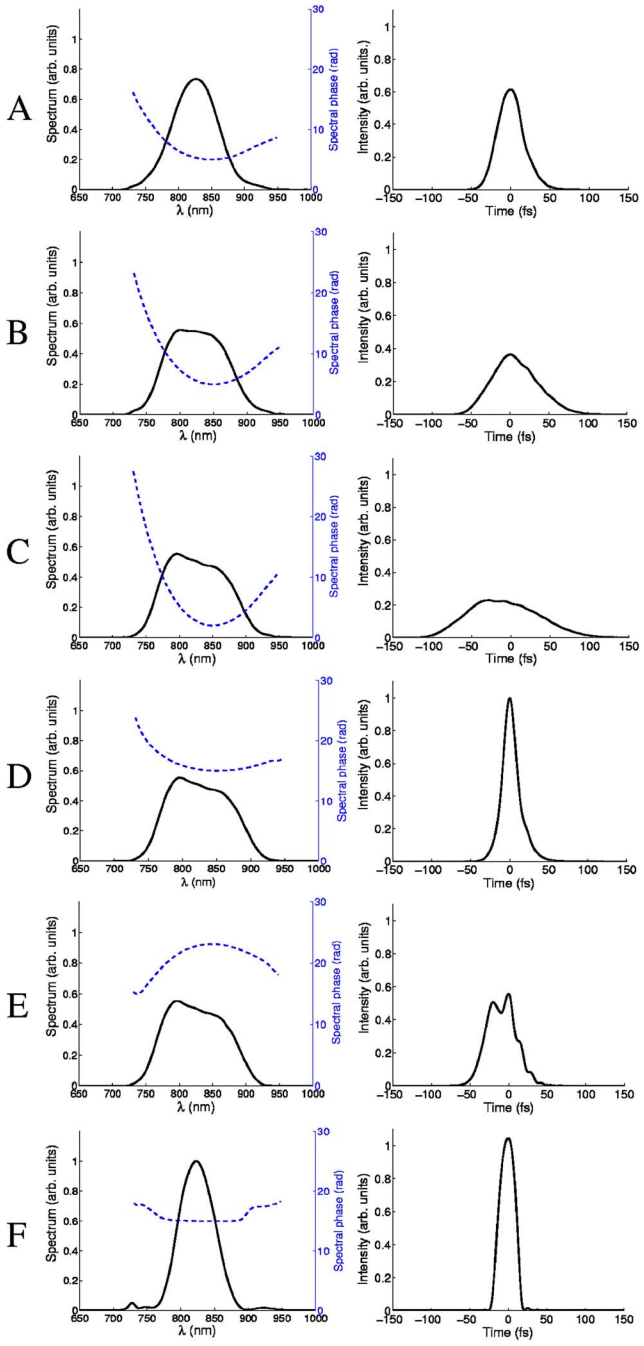

FIG. 5. (Color online) Spectra, phases, and temporal profiles corresponding to the reference points reported in Fig. 4.

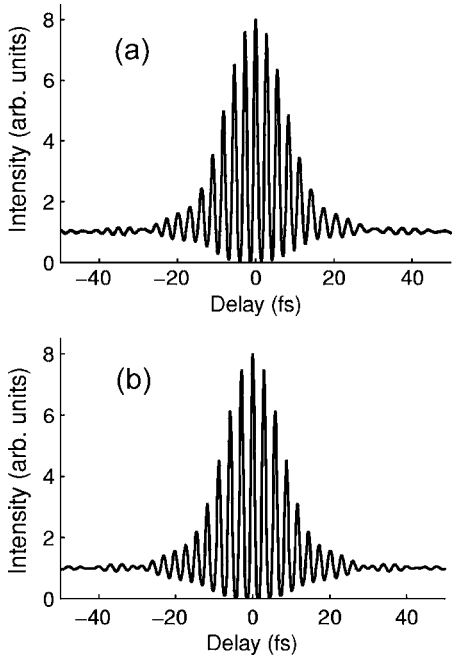

FIG. 6. (a) Measured and (b) simulated interferometric autocorrelation corresponding to the spectra of Fig. 3. In both cases, compensation of residual GDD is performed with an extracavity fused-silica prism pair.

reaches the silver mirror (point *D*), the acquired positive chirp is partially compensated for, while the spectrum remains unaffected, resulting in a shorter and more intense pulse. This is the point of maximum intracavity spectral width and minimum pulse duration. In contrast to the case of point *A*, when the pulse enters the crystal on its way back to the OC (point *E*), it is negatively chirped by a second passage in the prism sequence: nonlinear propagation now results in spectral narrowing and phase flattening until the pulse is transform limited at a depth of 3 mm within the crystal (point *F*). This is the point of minimum spectral width. As the pulse continues its way to the OC and goes back to the silver mirror, its spectrum is broadened, recovering its maximum width at points *C* and *D*. The pulse behavior described here confirms the dispersion managed model of mode locking [12], by showing the typical spectral and temporal *breathing* of DMS, in agreement with the experimental fact that spectra are broader when taken in the dispersive end of KLM lasers [8,16–18].

Furthermore, Fig. 5 shows that the pulse propagating in the cavity, while varying its spectral and temporal profiles, maintains a *smooth* spectral phase due to the joint action of SAM and SPM, which are able to wash out from the spectral phase the modulations inherent in the net intracavity GDD. This is in agreement with recent experimental results, where it was shown that operation of a broadband Ti:sapphire laser under strong Kerr-lens mode-locking conditions resulted in a smoothing of the spectral phase [2,3]. Once the pulse exits the cavity, such a well-behaved phase is suitable for further extracavity pulse compression. For the spectrum of Fig. 3, a pulse duration of 11 fs is obtained, in very good agreement with the experimental measurements, as shown in Fig. 6, and close to the Fourier-transform limit of both the simulated and measured spectra. This model also correctly predicts the observed reduction in spectral width with decreasing prism insertion. Since a decrease in prism insertion will increase the absolute value of the negative dispersion introduced by the prism pair, this will result in a displacement of the point having the narrowest intracavity spectrum (point *F* in Fig. 4) towards the OC, hence the observed reduction in the spectral width of the measured extracavity spectrum, as clearly shown in Figs. 7(a) and 7(b).

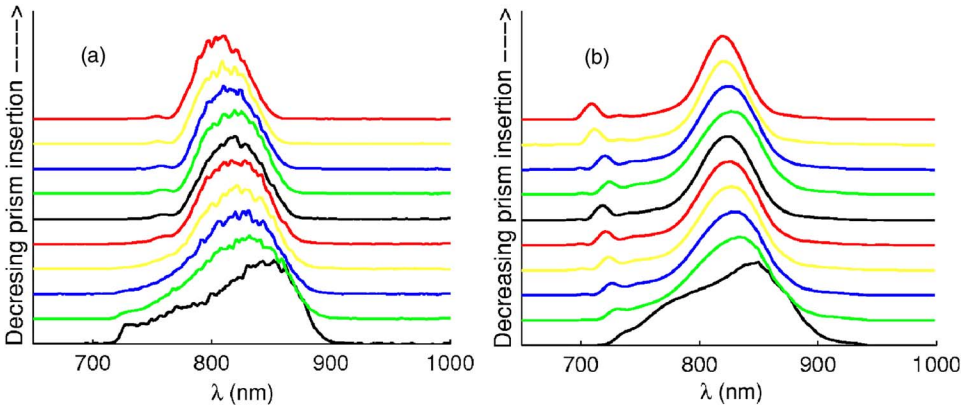

FIG. 7. (Color online) (a) Measured and (b) simulated spectral evolution as a function of prism insertion.

IV. CONCLUSION

In conclusion, we have developed what is to our knowledge the most realistic 1D numerical model of pulse evolution and propagation in a Kerr-lens mode-locked laser which accurately predicts the observed spectral shape, temporal width and energy of the pulses generated by an actual Titanium:sapphire oscillator. The obtained results are consistent with the dispersion managed model of mode locking, showing how the pulse acquires and preserves a *smooth* spectral phase as it propagates inside the cavity. A detailed experimental demonstration of intracavity pulse evolution as predicted by this model is presently under development.

ACKNOWLEDGMENTS

This work was partly supported by FCT Grant No. POCTI/FIS/48709/2002, Portuguese Ministry of Science, cofinanced by FEDER.

[1] H. A. Haus, IEEE J. Sel. Top. Quantum Electron. **6**, 1173 (2000).
[2] U. Morgner, F. X. Kärtner, S. H. Cho, Y. Chen, H. A. Haus, J. G. Fujimoto, E. P. Ippen, V. Scheuer, G. Angelow, and T. Tschudi, Opt. Lett. **24**, 411 (1999).
[3] T. Fuji, A. Unterhuber, V. S. Yakovlev, G. Tempea, A. Stingl, F. Krausz, and W. Drexler, Appl. Phys. A: Mater. Sci. Process. **77**, 125 (2003).
[4] P. F. Curley, Ch. Spielmann, T. Brabec, F. Krausz, E. Winter, and A. J. Schmidt, Opt. Lett. **18**, 54 (1993).
[5] I. P. Christov, M. M. Murnane, H. C. Kapteyn, J. Zhou, and Ch.-P. Huang, Opt. Lett. **19**, 1465 (1994).
[6] I. P. Christov, V. D. Stoev, M. M. Murnane, and H. C. Kapteyn, Opt. Lett. **21**, 1493 (1996).
[7] T. Brabec, Ch. Spielmann, and F. Krausz, Opt. Lett. **16**, 1961 (1991).
[8] F. Krausz, M. Fermann, T. Brabec, P. F. Curley, M. Hofer, M. H. Ober, C. Spielmann, E. Wintner, and A. J. Schmidt, IEEE J. Quantum Electron. **28**, 2097 (1992).
[9] C. Spielmann, P. F. Curley, T. Brabec, and F. Krausz, IEEE J. Quantum Electron. **30**, 1100 (1994).
[10] K. Tamura, E. P. Ippen, H. A. Haus, and L. E. Nelson, Opt. Lett. **18**, 1080 (1993).
[11] K. Tamura, E. P. Ippen, and H. A. Haus, Appl. Phys. Lett. **67**, 158 (1995).
[12] Y. Chen, F. X. Kartner, U. Morgner, S. H. Cho, H. A. Haus, E. P. Ippen, and J. G. Fujimoto, J. Opt. Soc. Am. B **16**, 1999 (1999).
[13] H. Haus and Y. Chen, J. Opt. Soc. Am. B **16**, 889 (1999).
[14] Q. Quraishi, S. T. Cundiff, B. Ilan, and M. J. Ablowitz, Phys. Rev. Lett. **94**, 243904 (2005).
[15] H. Crespo, M. V. Tognetti, M. A. Cataluna, J. T. Mendonça, and A. dos Santos (unpublished).
[16] Ch.-P. Huang, M. T. Asaki, S. Backus, M. M. Murname, and H. C. Kapteyn, Opt. Lett. **17**, 1289 (1992).
[17] M. T. Asaki, Ch.-P. Huang, D. Garvey, J. Zhou, H. C. Kapteyn, and M. M. Murnane, Opt. Lett. **18**, 977 (1993).
[18] B. Proctor and F. Wise, Appl. Phys. Lett. **62**, 470 (1993).